Simulations and field tests of pneumatic power regulation by valve control using short-term forecasting at the Pico OWC

Simulations and Field Tests of Pneumatic Power Regulation by Valve Control Using Short-term Forecasting at the Pico OWC

Kieran Monk[#*1], Daniel Conley[#2], Victor Winands[~3],
Miguel Lopes[*4], Qingping Zou[+5,] Deborah Greaves[#6]

[#]*School of Marine Science and Engineering,*
University of Plymouth
Plymouth, PL48AA, UK
[1]kieran.monk@plymouth.ac.uk
[2]daniel.conley@plymouth.ac.uk
[6]deborah.greaves@plymouth.ac.uk

[+]*Department of Civil and Environmental Engineering,*
University of Maine
Orono, ME 04469, USA
[5]qingping.zou@maine.edu

[*]*WAVEC - Offshore renewables*
Lisbon, 1400-119, Portugal
[1]kieran@wavec.org
[4]mlopes@wavec.org

[~]*Department of Civil Engineering*
Aalborg University
Aalborg, DK-9200, Denmark
[3]vw@civil.aau.dk

***Abstract*— Power production at the Pico OWC WEC has fallen significantly short of early theoretical projections. The main reasons for this that have been identified are: the collection of boulders in the chamber has reduced the water depth promoting wave asymmetry, a defect in the chamber front lip makes a pneumatic connection to the atmosphere at times resulting in pressure loss, and the maximum turbine rotational speed has been limited to below the optimum. In addition the turbulent flow shed from the Wells turbine under stall conditions causes significant stress in the mechanical system components resulting in accelerated fatigue and excessive noise emission. The constant need to maintain and recover fatigued components is an unsustainable drain on financial and human resources. In order to improve power production and reduce fatigue rate by minimising stall frequency and severity, a control strategy is considered to improve pneumatic power exposure to the turbine through relief valve control, using the existing infrastructure. Control decisions are made using the information obtained through short-term wave forecasting using an autoregressive model. Simulations of control are in good agreement with field test results obtained at Pico.**

***Keywords*— OWC, control, forecasting, wave energy, Pico, relief valve, Autoregression**

I. INTRODUCTION

Pico is one of a few full scale, grid connected, wave energy converters (WEC) in the world. It is a shore mounted oscillating water column type WEC located on the Portuguese island of Pico in the Azores archipelago. The plant has a chamber with a submerged opening to incident waves and the oscillating water surface inside the chamber from wave action acts as a piston to compress and expand the bound air pocket. This oscillating pressure head (relative to the atmosphere) creates a reciprocating flow through a duct housing a Wells turbine, which is connected to a doubly fed asynchronous generator. Fig. 1 shows the plant system configuration.

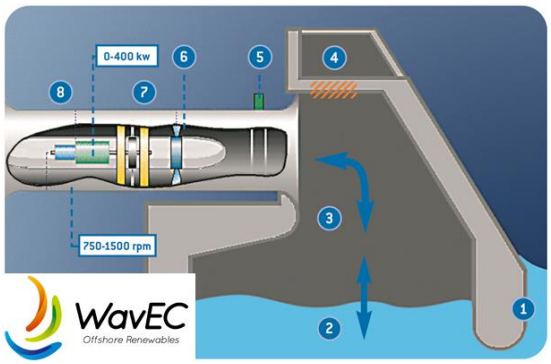

Fig. 1 Cross-sectional illustration of the Pico OWC system indicating; (1) the incident wave, (2) the chamber oscillation, (3) the bound air pressure chamber, (4) by-pass relief valve, (5) Main isolation valve, (6) Fast acting isolation valve, (7) Wells turbine, (8) Asynchronous generator.

The Wells turbine is self-rectifying. This avoids more complicated variable pitch turbines or air flow rectification options. However, one significant limitation of the Wells turbine is the stall effect. The relative angle of attack of the blades with respect to the driving air flow is the vector sum of both the turbine blade tip and driving air flow velocities. When the relative angle of attack exceeds a critical threshold the boundary layer separates leading to a loss of lift force and an increase in drag. In stalled conditions the pneumatic to mechanical power conversion efficiency reduces rapidly as flow separation spreads radially from the hub, with further increasing airflow rate. At full flow separation the transfer efficiency drops effectively to zero as seen in Fig. 2. As will be discussed later, air vortex shedding during stall interacts with the turbine and guide vanes and ducts, and increases system vibrations significantly, which increases the rate of mechanical fatigue (as shown in a related study).

Using stochastic methods when considering: the local wave climate at Pico (from monitoring), original design chamber water depth, specific system specification and turbine

characteristics, and by using an optimised power take off control curve, it was projected in [1] that that the Pico OWC should achieve power take-off averages greater than 90 (kW) for the majority of sea states at this locality. This was projected to reach averages of up to 190 (kW) in the most energetic sea states and average around 100 (kW) over all operational periods (annually). In reality the Pico plant achieves a maximum level of power take-off of about 60 (kW) (averaged over an hour) and an average of about 30 (kW) over all periods that are chosen for operation. The actual performance of the Pico plant is considered in [2]. This is a significant shortfall of about 70% when considering operational periods only (as selected by the plant operator). The short-fall would be greater still if all time periods were considered. Because of this the project is not commercially interesting at the present. However, as a functional full scale grid-connected device the project still present a unique and interesting platform for testing and research purposes.

Before proceeding further it is useful to discuss the Pico Wells turbine characteristics because these define the dominant mechanical system response. In [3], convenient non-dimensional equations (by the turbine angular velocity N) are provided for: chamber pressure head p_c, air mass flow rate $\dot{m}_t$ across the turbine and pneumatic to mechanical power transfer to the turbine P_a, as described respectively by;

$$\Psi = \frac{p_c}{\rho_0 N^2 D^2} \qquad \Phi = \frac{\dot{m}_t}{\rho_0 N D^3} \qquad \Pi = \frac{P_a}{\rho_0 N^3 D^5} \qquad (1,2,3)$$

where D is turbine diameter and ρ_0 is the density of air at atmospheric pressure.

These non-dimensional quantities allow the turbine characteristic curves (an essential element of the OWC system model) to be inspected in two dimensions. The characteristics for the Wells turbine used at Pico were found in [4] using a smaller scaled turbine in laboratory experiments and these are presented in Fig. 2. In particular it is noted that a rapid decline in pneumatic to mechanical power transfer occurs when the non-dimensional pressure exceeds the threshold $\Psi_{cr} = 0.067$.

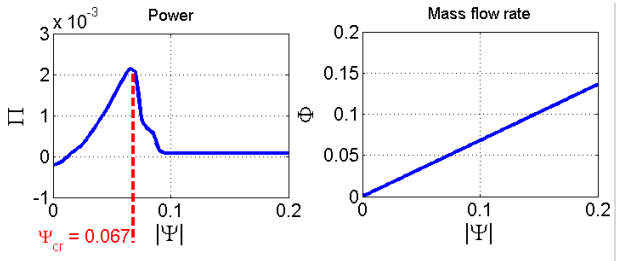

Fig. 2 From [4] the non-dimensional pressure Ψ vs (left) non-dimensional power Π transfer to the turbine and (right) non-dimensional mass flow rate of air passing the turbine, for the Pico Wells turbine.

The disparity between theoretical and achieved power production levels is at least in-part due to a number of deviations from the original optimised design methodology that were incurred in reality, as discussed in the following.

The boulder dam erected to protect the plant construction site was damaged by strong wave action and several thousands of cubic meters of rock debris were distributed near the plant site [5]. Much of this was subsequently removed but a significant proportion collected in the plant chamber making extraction difficult. This significantly reduced the water depth in the chamber and the area just up-wave of the plant. The change in water depth will likely affect the plants hydrodynamic transfer coefficients and frequency response as demonstrated in [6]. In addition, shallower water depths increase the wave shoaling effect, and ultimately produce a more asymmetric chamber pressure profile. Even if the variance in pressure is optimal over a wave cycle, wave asymmetry typically results in over-pressure for a portion of the positive chamber pressure head half wave cycle resulting in turbine stall, and under pressure for the negative pressure head half of the wave cycle. The result is poorer power transfer to the turbine compared to what could be achieved with a more symmetrical (about zero pressure head) pressure profile. The impact of this effect is clearly seen in the data and a typical example is presented in Fig. 3 which shows how the performance of the plant is directly and very strongly related to tidal elevation (degree of wave shoaling).

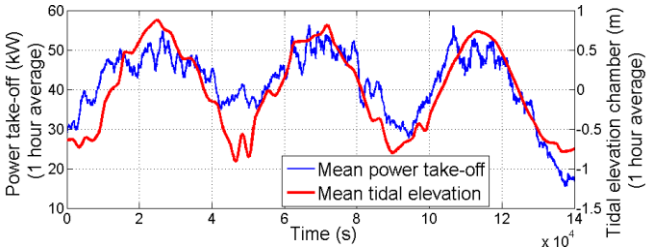

Fig. 3 Example relationship of mean power take-off and tide elevation, each data point gives the 1-hour average of the variable about the data time point.

The problem is exacerbated by a missing portion of the chamber front lip which has broken away, as shown in Fig. 4. This results in a passage opening between the chamber and the atmosphere during some wave troughs with the frequency increasing with increasing wave height and at lower tide positions. When the passage emerges from the water, chamber pressure head is lost momentarily and this causes a step in the pressure profile as shown in Fig. 4 reducing the proportion of time spent in the more optimal power transfer pressure region.

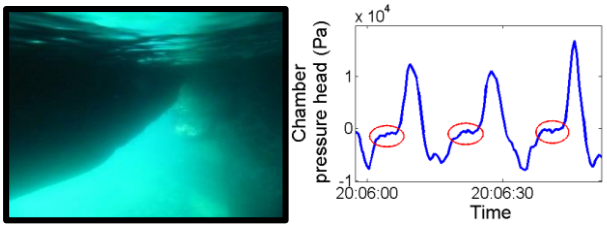

Fig. 4 (left) Missing section of chamber front lip that emerges during larger wave troughs with increasing frequency with lower tides, (right) example of chamber pressure modification due to missing section of chamber front lip

At present when the turbine angular velocity $N > 141\ (rads^{-1})$, high levels of power are taken off the generator which acts as a strong electro-magnetic break. This was implemented in reaction to a downgrade of the maximum handling capacity of the power electronics. Also, residual vibration velocities (measured at the turbine shaft bearings) enter the "unacceptable" ISO 10816 severity rating range when this imposed upper limit of N is exceeded. The long term consequences (accelerated fatigue) of running the machine in this range are not known. The rotational speed limit considered in [1] was $N = 157\ (rads^{-1})$ based on the physical limitations of the turbine as specified by manufacturers. This deviation presents another possible source for the short-fall in performance. The non-optimised power take-off control law currently used at the plant is shown in Fig. 5 and is compared to the theoretical optimum curve as described in [1].

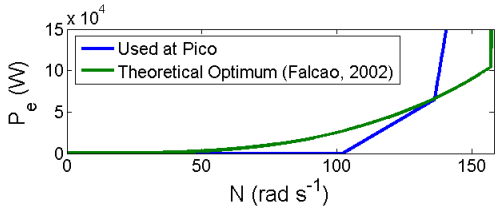

Fig. 5 Comparison of power-take off control law used at Pico and theoretical optimum as described in [1]

Turbine stall, as well as limiting the plant performance also causes other significant issues. The turbulent air shed from the turbine in stall conditions causes a significant increase in the system vibration velocities. For example, Fig. 6 shows the RMS vibration velocities measured at the atmosphere side turbine shaft bearing. When the residual vibrations (no aerodynamic loading) are removed from the mean vibrations (shown as a function of turbine rotational speed and non-dimensional pressure) a clear relationship can be seen between the point of stall onset $(\Psi = 0.067)$, the point of full separation $(\Psi \approx 0.01)$ and the vibrations levels above the residual. Vibration levels increase with further increase of Ψ.

High vibration levels cause stress requiring continual maintenance and repair to neutralise the resulting fatigue. The impact of turbine stall on component fatigue at Pico is considered in [7] where stresses on the turbine guide vanes from aerodynamic loading were measured and found to increase very sharply when the stall threshold is exceeded. It was concluded that the stress imposed by aerodynamic loading was the root cause of serious fracturing of the guide vane blades which forced the complete removal of the structure. Interestingly the chamber side guide vanes, exposed to turbulent flow loading during the negative pressure head half have cycle, are unaffected due to the less frequent and less severe stall in that direction (due to wave asymmetry). The constant need to repair stress-damaged components is a significant financial and human resource drain, and needs improving.

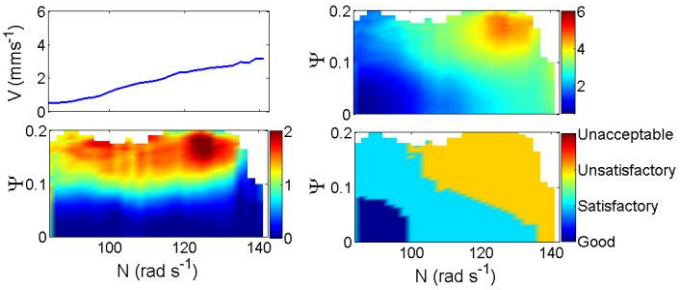

Fig. 6 RMS Vibration velocities (mms^{-1}) at the atmosphere side turbine shaft bearing. (top left) Residual mean vibration with no aerodynamic loadings. With positive pressure head; (top right) mean vibration velocities, (bottom left) difference between mean vibrations and residual vibrations, (bottom right) ISO 10816 vibration severity ratings of mean vibration velocities.

These issues could probably be corrected by: repairing the subsurface structural defects and dredging the boulders Also by restoring the original power electronics power capacity and further stiffening the turbo-generator support structure to suppress vibrations, would permit higher rotational speeds. However, very high cost is associated with each of these activities and the financial return from enhanced energy sales probably does not justified the expense. From a research perspective the main value of these interventions would be to try to attain a more Gaussian distribution of chamber pressure to validate the stochastic modelling approach given in [8].

Implementing a more optimal power take off curve has no cost and the third author is currently researching this topic. Another option for performance enhancement of OWCs with Wells turbines, that is potentially low cost and with significant research value, is the regulation and optimisation of chamber pressure, for greater pneumatic to mechanical power transfer to the turbine.

The objective of this study is to increase useful pneumatic power by controlling the relief valve to minimise periods of over-pressure that result in turbine stall. This is achieved from active relief valve control directed by short-term wave forecasting. Relief valve control (with this objective) will necessarily reduce the frequency and severity of turbine stalls, and a reduction in the rate of fatigue from vibrations should also be achieved.

II. Methodology

A logical sequence of steps needed to theoretically develop a WEC control strategy is given in the following and accomplished in subsequent sub-sections;

- Define an optimised basic control strategy to provide a base-line for quantifying any gains from advanced control.
- Develop a methodology for an advance control strategy.
- Create a model to test the performance of the proposed strategy and to further refine the methodology.
- If the control strategy is not passive a short-term wave forecast model needs to be developed and incorporated into the control portion of the system model.

A. *Relief valve control*

To extend the operational sea-state range of the plant there is an opening in the chamber roof with an adjustable aperture, as shown in Fig. 7. This acts as a by-pass pressure relief valve and can be used to modify chamber pressure. The value has a maximum square aperture of 1.69 $[m^2]$ and the aperture is controlled by a gate which is actuated by a hydraulic ram. At present, the rate of aperture adjustment is 4.5 $(\%/s)$ when closing and 3.8 $(\%/s)$ when opening.

Fig. 7 Picture of relief valve and aperture adjustment system

In [9] and [10] a relief valve control strategy is devised which requires a relief valve actuator system of high technical specification. As seen in Fig. 2, for the Pico wells turbine, a threshold non-dimensional pressure exists ($\Psi_{cr} = 0.067$) at which point the maximum possible power (at the specific turbine speed) is transferred to the turbine. By achieving $\Psi_{cr} = |\Psi|$ as quickly as possible with a zero valve aperture (after slack chamber pressure associated with the wave peak or trough) and then sustaining it for as long as possible through rapid subsequent aperture adjustments, a significant enhancement in power transfer to the turbine will ensue. To achieve control in this fashion a powerful and highly responsive relief valve aperture adjustment system, that is robust enough to withstand a high duty cycle, is required. Such a relief valve actuator system has yet to be developed. Utilising the existing relief valve aperture adjustment system at Pico some lower tech relief valve control strategies are considered in the following.

1) Basic relief valve control: As shown in [1] stochastic analysis suggests that for the Pico Wells turbine, without advanced relief valve control, the maximum mean non-dimensional power transfer to the turbine $\overline{\Pi}$ Is achieved when the standard deviation of non-dimensional pressure is $\sigma(\Psi) \approx 0.05$. This has been confirmed using operational data and the profile of $\overline{\Pi}$ vs $\sigma(\Psi)$ is shown in Fig. 8. Basic relief valve control at Pico is used to make small infrequent adjustments of the valve aperture to try to converge and maintain $\sigma(\Psi)$ with its optimum value, over time. This is the most basic option for pneumatic power regulation using relief valve control and will be referred to as $Basic_{RVC}$. The plant performance resulting from $Basic_{RVC}$ is used as an optimised base-line for evaluating any performance enhancements from more advanced relief valve control strategies.

2) Envelope relief valve control: Although not designed for the purpose, the existing relief valve system at Pico could be used to make more frequent aperture adjustments than $Basic_{RVC}$. Because of wave asymmetry the obvious option would be to try to optimise chamber pressure over a half wave cycle. However, it was found that this required too frequent valve aperture adjustments and ultimately caused over-heating of the hydraulic pump that feeds the valve adjustment ram. The next best time period to optimise pressure is the full wave cycle. This will incur far fewer aperture adjustment cycles, and is therefore more likely to be achievable in reality with the existing infrastructure at Pico.

To implement a valve control strategy of this type first a control evaluation parameter needs to be identified. Six 35-minute periods of real operational data with $T_p \approx 14\ (s)$, but with H_s ranging between 2 & 5 (m) were selected from the available data. The mean non-dimensional power transfer to the turbine $\overline{\Pi}_{T_p}$, as a function of the standard deviation of non-dimensional chamber pressure head, over a time period equal to the sea state peak period $\sigma_{T_p}(\Psi)$, was found for every data time instant of each data set. This is described by the equations 4 and 5, and the evaluation of the result is shown in Fig. 8;

$$\sigma_{T_p}(\Psi) = \sqrt{\frac{1}{T_p f_s}\sum_{l=1}^{k+T_p f_s}\left(\Psi(k+l) - \frac{1}{T_p}\sum_{l=1}^{k+T_p f_s}\Psi(k+l)\right)^2} \qquad (4)$$

$$\overline{\Pi}_{T_p} = \frac{1}{T_p f_s}\sum_{l=1}^{k+T_p f_s}\Pi(\Psi(k+l)) \qquad for\ k = 1,2,..L - T_p f_s \qquad (5)$$

where k is the data time point, $f_s = 2\ (Hz)$ is the data sampling frequency and L is the data set length.

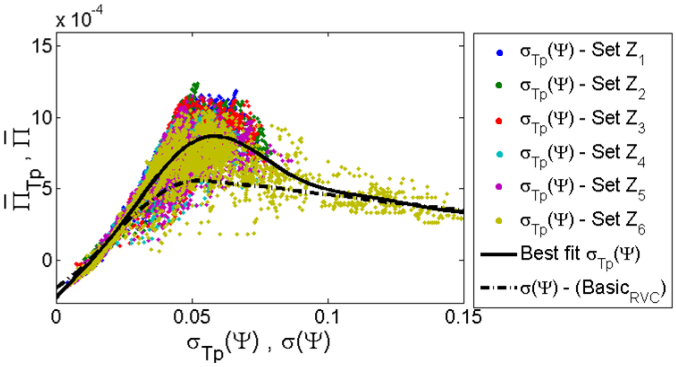

Fig. 8 Mean non-dimensional power transfer to turbine $\overline{\Pi}_{T_p}$ over a time period $T_p = 14\ (s)$ as a function of the standard deviation of chamber pressure over the same time period $\sigma_{T_p}(\Psi)$, for different selected data sets, with a line of best fit for the data sets combined. This is compared to the mean non-dimensional power $\overline{\Pi}$ over longer periods of time (equivalent to the length needed to define a sea state) as a function of the long term standard deviation of non-dimensional pressure $\sigma(\Psi)$ as found from stochastic analysis in [1].

As seen in Fig. 8, over an approximate wave cycle, and on average (as indicated by the line of best fit), a greater level of mean non-dimensional power transfer to the turbine $\overline{\Pi}_{T_p}$ results when $0.04 < \sigma_{T_p}(\Psi) < 0.08$ compared to $\overline{\Pi}_{max}$ achieved over longer time periods by optimising $\sigma(\Psi) \approx 0.05$. Higher value ($0.06 < \sigma_{T_p}(\Psi) < 0.08$) result in good power transfer but will incur more frequent and severe stalls which is un-desirable. As such optimising to the lower half of the range, namely $0.04 < \sigma_{T_p}(\Psi) < 0.06$, seems more appropriate. Of course, achieving the optimum $\sigma_{T_p}(\Psi)$ is only possible if the sea state is sufficiently energetic.

By steering $\sigma_{T_p}(\Psi)$ in to the optimum range rather than trying to always maximise $\overline{\Pi}_{T_p}$ the relief valve aperture will not adjust to minor fluctuations in the incident wave energy, thus reducing the valve duty cycle. Finally, to reduce relief valve adjustments further, the aperture closing rate is halved so that the valve aperture is not significantly decreased during shorter periods of lower incident energy, requiring a smaller subsequent increase in aperture for the next temporal period of higher incident energy. The maximum aperture rate of adjustment for the open stroke is maintained so that the valve can react quickly to any detected sharp increases in incident energy in order to vent over-pressure, minimising the likelihood of a severe stall occurring. Control in this fashion causes the relief valve aperture to track the wave envelope rather than reacting to shorter temporal fluctuations and as such this strategy will be referred to as $Envelope_{RVC}$.

The correlation in the relationship between $\overline{\Pi}_{T_p}$ and $\sigma_{T_p}(\Psi)$ (in Fig. 8) is not great and this is in part due to the varying degrees of wave asymmetry. High wave asymmetry results in a lower $\overline{\Pi}_{T_p}$ and vice versa. Also, it is because the time length to assess $\sigma_{T_p}(\Psi)$ is simply equal to the sea state peak period and not necessarily the actual wave period in question. As such, the evaluation of $\sigma_{T_p}(\Psi)$ might only span part of a wave cycle or a wave cycle and a part of the next. At any instance this might encompass a disproportionate degree of chamber pressure levels that result in higher or lower levels of mean power transfer to the turbine. The up-coming wave period could be predicted to find $\sigma_T(\Psi)$ but a wave period is difficult to define part way through a wave cycle and adds complexity to the procedure. However, this would probably be required for localities that do not experience such narrow banded wave spectra as the Pico site. This evaluation method (using peak period) on the other hand is very simple requiring no dedicated phase forecast (to evaluate the actual up-coming wave period) and promotes a simple and fast control procedure. Of course $Envelope_{RVC}$ requires a forecast of $\hat{\sigma}_{T_p}(\Psi)$ with horizon equal to T_p to function and short-term forecasting is considered later.

B. Wave to wire model

It is important to first validate and refine $Envelope_{RVC}$ and assess the potential enhancements in order to justify deployment. This can be achieved with a wave to wire power transfer model in the time-domain. Time-domain modelling is needed over the alternative which is stochastic modelling in the frequency domain, due to the further deviation from a Gaussian probability density of chamber pressure that necessarily results from relief valve control.

OWCs are probably the most intensively studied of all proposed WEC technologies and a wealth of theory exists. A solution for the transfer of excitation flow to chamber pressure in the time domain is given in [10], and this is directly applicable to the Pico OWC. The full derivation is lengthy and [10] should be consulted for more details, but the equation relating chamber hydrodynamics to chamber pressure is;

$$\frac{dp_c}{dt} = \frac{\gamma p_0}{V_0}\left[q_e + q_r - \frac{\dot{m}_t + \dot{m}_v}{\rho_0}\right] \tag{6}$$

where γ is the heat capacity ratio of air, ρ_0 the density of air at atmospheric pressure, $\dot{m}_t$ the mass flow rate of air past the turbine;

$$\dot{m}_t = v_x A_D \rho_c \tag{7}$$

and $\dot{m}_v$ the mass flow of air through the relief valve;

$$\dot{m}_v = \rho_0 \mathrm{k}_v A_v C_d \mathrm{sign}(p_c)\left(\frac{2|p_c|}{\rho_o}\right)^{1/2} \tag{8}$$

where v_x is the air flow rate passing the turbine, A_D the turbine duct cross sectional area, ρ_c the chamber air density, $p_c$the chamber pressure head, k_v the relief valve aperture state (0 for closed 1 for open) A_v the maximum valve aperture area and C_d the discharge coefficient.

Following from [11] , q_e is the excitation flow rate which is the rate of change of the air volume in a system completely open to the atmosphere as described by;

$$q_e = -\frac{dV_{open}}{dt} = \frac{d(\eta_e y_H x_H)}{dt} \tag{9}$$

with V_{open} being the open system air volume, η_e the excitation surface elevation which is conceptual only and refers to the hypothetical situation where the surface elevation is perfectly flat at all locations inside the chamber and y_H is the internal chamber width and x_H internal chamber length.

q_r is the rate of change of chamber air volume resulting from radiation wave generation from chamber pressure;

$$q_r = \int_{-\infty}^{t} \mathrm{g}_r(t-\tau)p(\tau)d\tau \tag{10}$$

The combination of both flow components gives the total rate of change of air volume V in a closed system.

$$-\frac{dV}{dt} = q_e + q_r \tag{11}$$

(See for example [12] for a more detailed description)

g_r is the chamber pressure memory function (see [9] for more details) and is described by;

$$g_r(t) = \frac{2}{\pi}\int_{-\infty}^{\infty} B(\omega)\cos(\omega t)d\omega \quad (12)$$

where $B(\omega)$ is the radiation conductance which was found using BEM analysis in [13]. Alternatively an analytical solution for an approximation of the Pico situation is given in [14] and this is used in this study;

$$B = -2\frac{2\omega\mu y_H}{\rho_w g k\left(1+\frac{\omega^2}{g}\operatorname{csch}^2(kh)\right)}\sin^2(kx_H) \quad (13)$$

where k is the wave number and h is the water depth

The wave to wire system model is then completed utilising the turbine characteristic curve presented in [4] and shown in Fig. 2 and the following power balance equation;

$$P_a = IN\frac{dN}{dt} + P_e + P_b + P_{el} \quad (14)$$

where P_e is the electrical power take-off (a function of N), P_b is the power dissipation from bearing friction which is approximated theoretically in [1], P_{el} is power loss due to the generators mechanical to electrical conversion efficiency and was found to be $P_{el} = {P_e}^{0.8}$ (approximately and when P_e is in Watts) and finally I is the moments of inertia of the rotating elements.

The time-domain model presented requires that the chamber excitation flow be known q_e (or indeed the surface elevation excitation flow η_e) as an input to drive the model, as well as the recent chamber pressure history as part of the memory function g_r. To gain a time series of q_e one could synthesise an incident wave time series, or attempt to sample the incident wave information by extracting it from the superposition formed with reflected and radiated propagating up-wave from the plant. After, the hydrodynamic transfer coefficients given in [13] could be used to predict the hydrodynamic response in the chamber. However, without updating the hydrodynamic transfer coefficients (to the structural and bathymetric changes that have occurred) these methods will not resolve the intricacies related to the non-uniform water depth and structural defects. An alternative is to rearrange equation 6 to make q_e the subject and then to calculate it using the sampled: chamber pressure, pressure history, relief valve aperture, turbine rotational speed and tide position. Of course, without modification the calculated q_e time-series will yield the same time series of p_c that was used to calculate q_e in the first place. However, if modifications to the system (i.e. from relief valve control) are implemented in the model, the systems response to these changes can be simulated from the data derived time-series of q_e, yielding a different p_c.

Once the transfer from excitation flow to pressure has been found the system response, namely the turbine angular velocity, can be found using the power balance described by equation 14, but with dN/dt being the subject.

To validate the model presented in [10] a 12-hour period of data was selected for its strong variability in chamber sea state with H_s transitioning between 2 and 4 meters and T_p transitioning between 11 and 14 seconds. The model was tasked with simulating the system response in terms of turbine rotational speed and electrical power take off. The statistical performance of the model over this time period is presented in Table I. The model performance is evaluated by the mean absolute error and mean squared error in turbine angular velocity N (in radians per second) when compared to the recoded values from operational data. Also the mean error of electrical power take-off is given as a percentage of the original recoded value.

TABLE I
STATISTICAL ASSESSMENT OF MODEL PERFORMANCE

$MAE(N)$	$MSE(N)$	$ME(P_e)$
1.63	4.38	+0.03%

As seen in Table I the model accuracy is quite good which (amongst other aspects) validates (in-part) the turbine characteristic curve found for the small scaled version of the Pico Wells turbine [4]. For completeness and for the readers benefit an example time series comparing the simulated and recorded N and P_e is presented in Fig. 9.

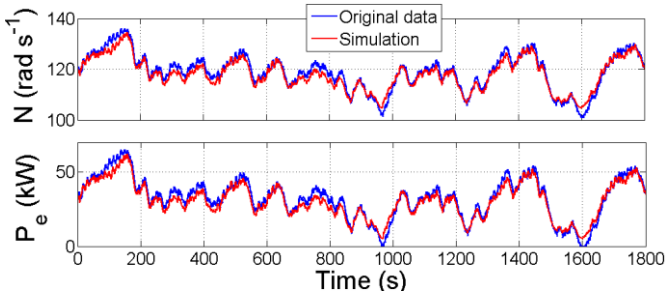

Fig. 9 Example time series comparing model prediction of turbine angular velocity and power take-off (red), and the recoded values (blue).

C. Short-term forecasting

The $Envelope_{RVC}$ requires a short term forecast of the chamber excitation flow $\hat{q}_e$ or its conceptual equivalent the excitation surface elevation $\hat{\eta}_e$ (as described by equation 9). $\hat{q}_e$ is used to model (in real time) the resulting chamber pressure in order to predict $\sigma_{T_p}(\Psi)$ and then to decide how best to modify this through valve aperture adjustments. A forecast with horizon equal to sea state peak wave period is needed.

A number of forecast models were investigated and these include models that use the information obtained exclusively at the device; Auto-Regressive (AR) and Non-linear Auto-Regressive (NAR) using non-linear functions optimised through Artificial Neural Network (ANN) error minimisation. Also, models that utilise information obtained at the device in combination with information obtained up-wave of the device

(with lead time) as an exogenous input (single point hydrostatic pressure readings measured 60 meters up-wave); Auto-Regressive with eXogenous input (ARX), Non-linear Auto-Regressive with eXogenous input ($NARX$), are considered. In addition, an extension of the ARX was considered which uses a second AR model to first forecast the exogenous input to allow an infinite forecast length of the ARX model, which we call the ARX_{AR} model. Without this the ARX reverts to the AR model when the lead time, defined by the wave travel time between the up-wave sensor location and the plant expires (the same is true for $NARX$ and NAR, respectively). Finally, a Finite impulse response model (FIR) which considered both measurements at the device and up-wave with lead time in the training phase, but only up-wave measurements in the forecasting phase, is considered.

The best forecast accuracy (especially at longer horizon times) was found to be achieved with the ARX_{AR} followed by the $NARX$ and ARX (being about equal showing non-linearity is small or more probably it is uncharacterisable), then by the AR and NAR (again being about equal), and marginally worse was the FIR. However, the; ARX_{AR}, $NARX$ and ARX, were discarded because the level of performance enhancement relative to the AR and NAR models, did not justify (in this application) the cost and potential for failure associated with an up-wave sensor deployment (with real-time data connection with the plant). Because of the reduced computational expense and reduced susceptibility of training instability the AR was found to be favourable over the NAR. Unfortunately, mathematically describing all forecast models types investigated is too lengthy. As such only the AR forecast model description and performance analysis (which was selected for further investigation in this study) is presented. The formulation of some of the forecast models considered can be found in [15].

The Auto-Regressive (AR) forecast model as described in [13], [16], [17] and [18] for example, assumes that a measurement made at the device is linearly dependent on a number n_a of the past measurements made at the device (regressors), each weighted by a dedicated regression coefficient a_j, plus an error ε. In this case the target variable is the chamber excitation surface elevation η_e (although q_e could be used to equal effect) and the AR model is defined as;

$$\eta_e(k) = \sum_{j=1}^{n_a} a_j \eta_e(k-j) + \varepsilon(k) = \hat{\eta}_e(k) + \varepsilon(k) \qquad (15)$$

where k is the data time.

The optimum model coefficients a_j that minimise the error need to be found. Their values are determined using a batch training data set of length L with a least squares minimisation of the cost function J which is the 1-step ahead error variance;

$$J = \sum_{k=n_a+1}^{L} (\eta_e(k) - \hat{\eta}_e(k))^2 = \sum_{k=n_a}^{L} \varepsilon(k)^2 \qquad (16)$$

After the optimum regression coefficients a_j are found the one step ahead prediction is given by;

$$\hat{\eta}_e(k+1) = \sum_{j=1}^{n_a} a_j \eta_e(k-j+1) \qquad (17)$$

For a multi-step ahead prediction, the forecast model is closed in a loop so that the one step ahead prediction is fed back to the input to become the most recent data point for the next iteration (the oldest input is discarded so that the input signal has constant length). This gives the two step ahead prediction and successive iterations in this fashion can be made to give a forecast with unlimited horizon;

$$\hat{\eta}_e(k+l) = \sum_{j=1}^{n_a} a_j \eta_e(k-j+l) \qquad (18)$$

where on the right side of the equation $\eta_e = \hat{\eta}_e$ when $j < l$

In [17] and [15] the AR model considered achieved exceptional forecast accuracy of surface elevation (essentially perfect for a wave cycle) in the different case studies. This was achieved by first pre-processing the data using a non-causal zero phase (forward and backward filter pass in time) low-pass filter before training and querying the AR model input data. This technique is not achievable in on-line applications because future data needs to be known in order to effectively implement the zero-phase filter. We find that using a casual filter (single forward filter pass in time, a range of IIR and FIR were considered) that is realisable in on-line applications, results in a delay in the forecast which when removed effectively counteracts any improvements in the forecast accuracy gained from the filtering process. As such the forecasting accuracy using unfiltered data is representative of the best that is achievable in an on-line application.

TABLE II
SIGNIFICANT WAVE HEIGHT, PEAK PERIOD AND ENERGY PERIOD OF DATA SETS USED TO EVALUATE SHORT-TERM FORECAST MODEL PERFORMANCE

	$Z_{1,1}$	$Z_{1,2}$	$Z_{2,1}$	$Z_{2,2}$	$Z_{3,1}$	$Z_{3,2}$
H_s	2.0	2.1	2.5	2.4	3.1	3.2
T_p	13.5	14.2	13.5	14.2	13.5	13.5
T_e	13.2	13.6	13.3	13.5	13.4	13.2
	$Z_{4,1}$	$Z_{4,2}$	$Z_{5,1}$	$Z_{5,2}$	$Z_{6,1}$	$Z_{6,2}$
H_s	3.6	3.6	4.0	4.1	4.8	4.8
T_p	13.5	14.2	13.5	15.1	13.5	15.1
T_e	13.6	13.4	13.1	14.5	14.0	14.3

To assess the performance of the AR model, 6 data set pairs (12 sets in total, and un-filtered) spanning a broad range of chamber significant wave heights (as described in Table II), were selected from the available operational data. Each data set Z in the data set pair was 35 minutes in length (relevant to defining a sea state) and were concurrent in time. The first data set (in time) of the set pair was used to train the AR whilst the unseen second data set of the pair was used to query the trained AR. This is done to insure no over-fitting had occurred. Optimisation analysis revealed that in this

application an AR model order of n_a = 50 (data sampled at 2 Hz) achieved the greatest accuracy but this was a marginal improvement compared to other model order numbers except for very small values ($n_a < 8$).

The model performance is assessed in terms of the GOF index (equation 19) as shown in Fig. 10 which the reader might find useful because a cross comparison can be made with the results presented in [17] and [15].

$$GOF_l = 100 * \left(1 - \frac{\sqrt{\sum_{k=n}^{L-l}(\eta_e(k+l) - \hat{\eta}_e(k+l))^2}}{\sqrt{\sum_{k=n}^{L-l}\eta_e(k+l)^2}}\right) \quad (19)$$

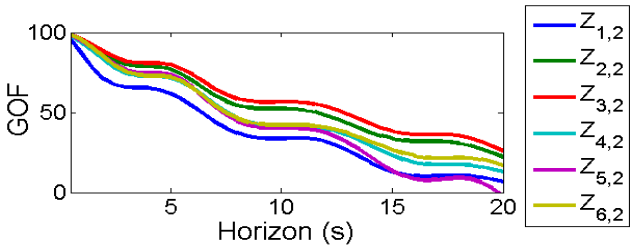

Fig. 10 Assessment of AR forecast accuracy of $\hat{\eta}_e$ in terms of the GOF index

From Fig. 10 it is seen that in all cases a fairly steady decline in forecast accuracy, as described by the GOF index, results from an increase in forecast horizon. GOF is strongly influenced by the forecast accuracy of both phase and amplitude. Further analysis revealed that the amplitude error does not depreciate much further after 6 (s) whilst the forecast phase accuracy continues to decline with increasing horizon.

III. Results

In this section, we will evaluate numerically the potential performance of $Basic_{RVC}$ and $Envelope_{RVC}$ using a numerical model in the time domain, whilst incorporating a realisable short term forecast for the chamber excitation surface elevation. The results will then be validated with field test results obtained whilst using the control strategies.

A. Simulations

The performance of each control strategy, using a forecast that is reliable on-line, was assessed using a numerical wave-to-wire system model in the time domain as described by equation 6 and 14. All available operational data over the time period 09/10/2014 to 26/11/2014 was selected to drive the model because of the high degree of sea state variability during this time. This data was divided into 30 minute periods which provided 1240 unique data sets (26 days in total) after the sea states with $H_s \leq 1.5$ were discarded (typically no net power production or finical gains countered by reactive power consumption costs). The total number of occurrence of each state is given in Fig. 11.

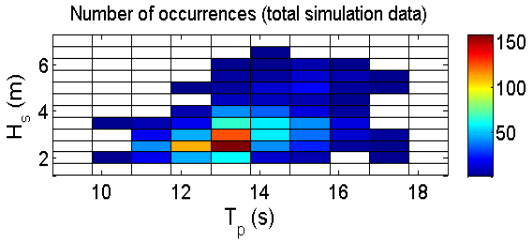

Fig. 11 total number of occurrence of chamber sea state for data sets used in mid-term relief valve control simulations

The simulation of $Basic_{RVC}$ which attempts to achieve $\sigma(\Psi) \approx 0.05$ valve control was implemented in the following way. Every 15 minutes, $\sigma(\Psi)$ was found for the past 15 minutes. If $\sigma(\Psi) < 0.048$ the relief valve aperture would be decreased by 5% in order to increase $\sigma(\Psi)$ over and the next 15 minute period, and vice versa if $\sigma(\Psi) > 0.052$ the relief valve aperture would be increased by 5%. This was done to try to continuously converge with the optimum $\sigma(\Psi) \approx 0.05$ (as shown in Fig. 8). This was found to be a very effective way of achieving $\sigma(\Psi) \approx 0.05$ and this reflects how $Basic_{RVC}$ is performed in reality at Pico. The simulation results of $Basic_{RVC}$ provide an optimised base-line for comparisons with $Envelope_{RVC}$.

For the simulation of $Envelope_{RVC}$, at each data time step k, the chamber excitation surface elevation is predicted using the AR model which provides $\hat{\eta}_e(k+l)$ (for $l = 1,2,\dots,T_p f_s$). The resulting chamber pressure (if $\mathrm{k}_v(k)$ were kept constant) is modelled in real-time, which allows $\hat{\sigma}_{T_p}(\Psi)$ to be predicted. If it is projected that $\hat{\sigma}_{T_p}(\Psi) < 0.04$, the relief valve aperture is set to decrease at a rate of 2.25 $(\%/s)$. If it is projected that $\hat{\sigma}_{T_p}(\Psi) > 0.06$ the relief valve aperture is set to increases at a rate of 3.8 $(\%/s)$. Finally, if $0.04 < \hat{\sigma}_{T_p}(\Psi) < 0.06$ the current relief valve aperture is maintained $\mathrm{k}_v(k) = \mathrm{k}_v(k+1)$. The AR model, used to ultimately predict $\hat{\eta}_e$, was trained using the data contained in the data set that preceded (in time) the data set driving the simulation, to reflect reality.

The simulated mean performance of each control strategy in terms of mean power take-off as a function of sea state (from chamber excitation surface elevation), is presented in the power matrices in Fig. 12.

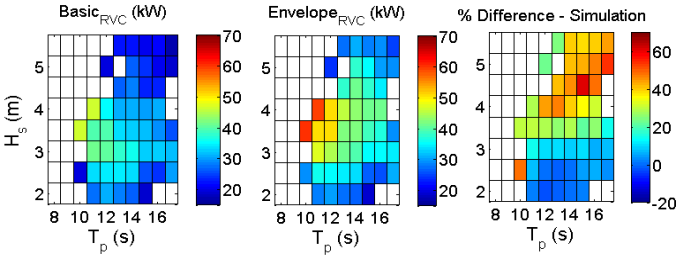

Fig. 12 Power take-off matrices comparing the performance of the different relief valve control strategies.

Table III gives the percentage difference between mean values resulting from $Basic_{RVC}$ and $Envelope_{RVC}$, for: power take-off and the proportion of time spent in excess of the stall

severity threshold bands, which we have simply defined from inspection of Fig. 6.

TABLE III
SIMULATED POWER TAKE-OFF AND PROPORTION OF TIME SPENT IN EXCESS OF STALL SEVERITY THRESHOLDS RESULTING FROM $Envelope_{RVC}$ AS A PERCENTAGE OF THAT RESULTING FROM $Basic_{RVC}$

$\%\ Differece\ vs\ Basic_{RVC}$	$Envelope_{RVC}$
$\bar{P}_e\ (kW)$	+15.4
$\Psi > 0.068\ \ (\%\ time)$	-4.9
$\Psi > 0.1\ (\%\ time)$	-24.4
$\Psi > 0.125\ (\%\ time)$	-43.7
$\Psi > 0.15\ (\%\ time)$	-56.8
$\Psi > 0.175\ (\%\ time)$	-59.4

As seen in Fig. 12, for medium to high energy sea states there is a reasonable amplification of power take-off using $Envelope_{RVC}$, with an increase of 15% for the data period considered. As seen in Table III the frequency of more severe turbine stalls is dramatically reduced. It should be noted that the simulation analysis only covers a period of one month (due to the significant computational expense) and the annual performance enhancement ratios are likely to be different and this requires more extensive analysis.

B. Field tests

The relative performance enhancements projected by the numerical simulations are reasonably significant but require validating with field test results. To evaluate the performance of $Envelope_{RVC}$ relative to $Basic_{RVC}$, the two control strategies were deployed in alternation for periods of 1 hour 15 minutes, for at least 7.5 hours (three sets under each control strategy). The last one hour of recoded data under each control strategy was logged and used for the results whilst the first 15 minutes of each test series segment was discarded. This time was considered as a generous transition period between the two routines to allow the system to settle into the new mode of control.

In total 11 test series were performed which covered a reasonable range of sea state conditions. It was hoped that testing would encompass the full range of possible sea state conditions but unfortunately due to a short circuit in the generator, testing of $Envelope_{RVC}$ ended abruptly.

To compare field test results of $Envelope_{RVC}$ and $Basic_{RVC}$, with the numerical model projections, each completed 1 hour field test result was collected into data bins based on chamber sea state characteristics H_s and T_p and tidal elevation, in the data bin interval of 0.5 (m), 1.0 (s) and 0.5 (m), respectively. The average of all data sets that fall into each data bin provided the final result. Tide elevation was included in the data division because in both the simulations and real test results it was found that tide had a significant influence on the performance of $Envelope_{RVC}$ (relative to $Basic_{RVC}$). This is due to the level of wave asymmetry from shoaling with $Envelope_{RVC}$ performing best with lower wave asymmetry associated with higher tidal elevations.

Fig. 13 presents the percentage difference between the electrical power take off $\bar{P}_e$ projected from the simulations of the $Envelope_{RVC}$ and $Basic_{RVC}$ strategies (blue line) for all simulation data sets arranged chronologically. The percentage difference between the two strategies, from field test results, is also given (Red dots) for the points having the same chamber sea state and tidal elevation.

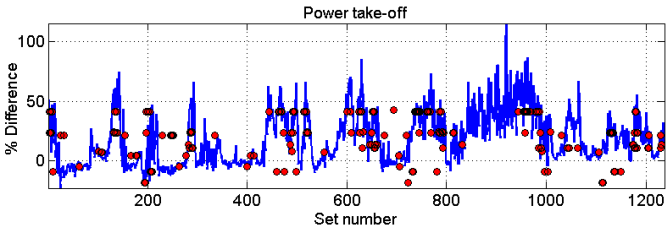

Fig. 13 Comparison of percentage difference in power take off between $Envelope_{RVC}$ and $Basic_{RVC}$ from simulations (blue line) and the mean value from field tests at times when a match in H_s, T_p and tide elevation occurs.

To provide an alternative analysis the field test results are presented in a more typical power matrix format in Fig. 14. In this case tidal elevation is not considered in the data division, and this can be compared to the simulation results given in Fig. 12 (the colour scaling is equal)

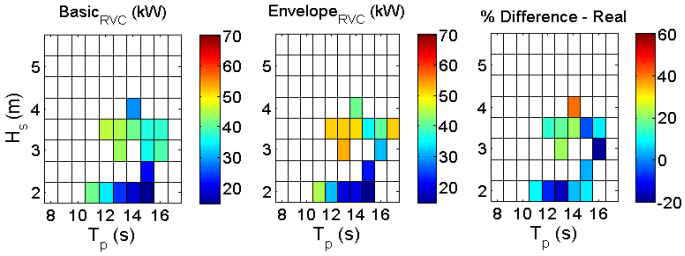

Fig. 14 Comparison of mean power take-off (left) $Basic_{RVC}$ and (middle) $Envelope_{RVC}$, for all field-test subsets that fall in to the identified data bin intervals for H_s and T_p.

As seen in Fig. 13, although only a limited number of field test data points exist, and with a few outliers, the achieved percentage difference in power take-off for the different sea states and tide positions, generally exhibit good agreement with the corresponding projections from the proposed numerical model and relief valve control characterisation therein. The projected reductions in turbine stall were also found to be accurate but there is not enough space to properly present this analysis.

As a final point of validation, the data obtained during one of the field test periods using $Envelope_{RVC}$, was simulated numerically to directly compare the real and numerical projections of the system response to control. In Fig. 15 a sample times series of recoded and simulated: relief valve aperture state k_v, turbine angular velocity N and electrical power take off by the generator, are compared. It is seen that the real and simulation results are generally in very good agreement. What is particularly interesting is how well the relief valve aperture tracks agree, despite the mildly chaotic nature of the problem. This shows that the characterisation of the rate of aperture adjustment and response time, were adequate.

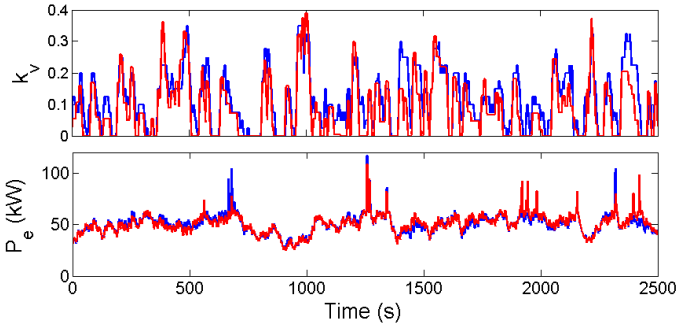

Fig. 15 Example time series comparing real data and simulations of: (top) relive valve aperture state, (middle) rotational speed, (bottom) Power take off

IV. Conclusions

A simple control strategy was developed to regulate turbine pneumatic power exposure at the Pico OWC to improve the performance by increasing power production and reducing the frequency and severity of turbine stall. This was achieved using only the rudimentary equipment available.

Control decisions are based on realisable short-term wave forecasts from an autoregressive model requiring plant side measurements exclusively.

The mid-term (one month in autumn) performance under the proposed control strategies was evaluated using a wave to wire power transfer model in the time-domain. By modifying and optimising the chamber pressure variance over a length of time equal to the sea state peak period, an increase in power production of 15% (compared to the basic control strategy and for the period considered) and significant reductions in the frequency of the severest turbine stalls, were projected for the period considered. The simulated performance projections from numerical modelling of the envelope relief valve control strategy were compared to a limited number of field test results obtained using the same control strategy, and generally good agreement was found.

In summary this study demonstrates that with basic equipment and minimal investment notable performance enhancements of a full-scale wave energy converter can be achieved using short-term wave forecasting using plant side data exclusively. Only a small selection of the results from this research are presented and the remainder will be disseminated in near future.

Acknowledgments

The first author would like to acknowledge the MARINET funding network which in-part financially supported this research. WAVEC – offshore renewables for providing unrestricted access to the Pico plant and data, Plymouth University for supporting this PhD programme, and the third author for plant side technical support.

References

[1] A. F. d. O. Falcão, "Control of an oscillating-water-column wave power plant for maximum energy production," Applied Ocean Research, vol.24, no. 2, pp. 73–82, Apr. 2002.," *Applied Ocean Research,* vol. 24, no. 2, p. 73–82, 2002.

[2] A. Pecher, I. L. Crom, J. P. Kofoed, F. Neumann and E. d. Brito-Azevedo, "Performance assessment of the Pico OWC power plant following the EquiMar methodology," in *International Offshore and Polar Engineering conference*, Maui, 2011.

[3] S. L. Dixon, Fluid Mechanics, Thermodynamics of turbomachinery, 3 ed., Oxford: Pergamon, 1978.

[4] L. M. C. Gato, V. Warfield and A. Thakker, "Performance of a high-solidarity wells turbine for an OWC wave power plant," *ASME Journal of Energy Resources Technology*, vol. 118, pp. 263-268, 1996.

[5] "European wave energy pilot plant on the island of Pico, Azores, Portugal. Phase two: Equipment," JOR3-CT95-0012, Contract, Lisbon, 1999.

[6] D. Ning, J. Shi, Q. Zou and B. Teng, "Investigation of hydrodynamic performance of an OWC (Oscillating water column) wave energy device using a fully nonlinear HOBEM (higher order boundary element method)," *Energy*, p. in press, 2015.

[7] M. Vieira, L. Reis and A. Sarmento, "Failure Analysis of the Guide Vanes of the Pico Wave Power Plant Wells Turbine," in *Sixth International Conference on Engineering Failure Analysis*, Lisbon, 2014.

[8] A. F. d. Falcao and R. J. A. Rodrigues, "Stochastic modelling of OWC wave power plant performance," *Applied Ocean Research*, vol. 24, pp. 59-71, 2002.

[9] A. F. d. O. Falcão and P. A. Justino, "OWC wave energy devices with airflow control," *Ocean Engineering*, vol. 26, no. 12, p. 1275–1295, 1999.

[10] A. F. d. O. Falcao, L. C. Vieira, P. A. P. Justino and J. M. C. S. Andre, "By-pass air-valve control of an OWC wave power plant," *Journal of Offshore Mechanics and Arctic Engineering*, pp. 205 - 210, 2003.

[11] D. V. Evans, "Wave power absorption by systems of oscillating surface pressure distributions," *Journal of Fluid Mechanics* , vol. 114, p. 481–499, 1982.

[12] J. Falnes, Ocean waves and oscillating systems, 1 ed., Cambridge: Cambridge University press, 2002.

[13] A. Brito-Melo, T. Hofmann, A. J. N. A. Sarmento, A. Clement and G. Delhommeau, "Numerical modelling of OWC-shoreline devices including the effect of surrounding coastline and non-flat bottom," *Journal of Offshore and Polar Engineering*, vol. 11, no. 2, p. 147–154, 2001.

[14] A. J. N. A. Sarmento and A. . F. d. O. Falcao, "Wave generation by an oscillating surface-pressure and its application in wave energy extraction," *Journal of Fluid Mechanics*, no. 150, p. 467–485, 1985.

[15] F. Paperella, K. Monk, V. Winands, M. Lopes, D. Conley and J. V. Ringwood, "Up-wave and autoregressive methods for short-term wave forecasting for an oscillating water column," *IEEE Transactions on Sustainable Energy*, vol. 6, no. 1, pp. 171-178, 2015.

[16] U. A. Korde, M. P. Schoen and F. Lin, "Time domain control of a single mode wave energy device," in *11th International Offshore and Polar Engineering*, Stavange, 2001.

[17] F. Fusco and J. V. Ringwood (b), "Short-term wave forecasting for real-time control of wave energy converters," *IEEE Transactions on Sustainable Energy*, vol. 1, no. 2, pp. 99-106, 2010.

[18] B. Fischer, P. Kracht and S. Perez-Becke, "Online-algorithm using adaptive filters for short-term wave prediction and its implementation," in *4th International Conference on Ocean Energy*, Dublin, 2012.